scientific reports

OPEN

Numerical simulation of water and salt transport during the re-injection process of farmland drainage

Siyu Chen[1,2], Ke Yang[2], Xu Zhang[2], Wangyang Zhang[2], Yuxiu Chen[2], Zijie Sang[2] & Ge Zhang[1,2]✉

The strategic reuse of agricultural drainage water presents a viable solution to address the growing disparity between water supply and demand in irrigated regions, with Soil Aquifer Treatment (SAT) systems demonstrating significant potential for water quality enhancement. However, the operational efficacy of SAT during drainage water recharge may be compromised by two principal factors stemming from compositional complexity: system clogging risks associated with improper management protocols or potential groundwater contamination through pollutant migration pathways. Through controlled laboratory experiments and systematic data analysis, this study revealed solute transport mechanisms in SAT simulated soil columns. Complementary HYDRUS-1D modeling further quantified the impacts of soil texture gradations and initial infiltration salinity on recharge system performance and subsurface environmental safety. The experimental results demonstrate that: (1) Media with fine-coarse particle gradation exhibited peak solute retention efficiency, and showed positive correlation with infiltration salinity. (2) Optimal gradation configuration requires salinity threshold control ≤ 1.3 g/L.

Freshwater scarcity, exacerbated by agriculture's predominant role in global water withdrawals (accounting for approximately 70%), necessitates the development of innovative water reuse strategies[1] In irrigation-dependent ecosystems, agricultural drainage water—a consequential byproduct of intensive cultivation—presents a dualistic challenge: while it represents a potential resource (e.g., for supplemental irrigation, as demonstrated in India's Punjab region[2] and treated wastewater reuse initiatives in Greece[3], it also poses significant environmental risks due to contaminants, including salts, heavy metals, and excess nutrients[4–6]. Direct reuse without adequate treatment exacerbates soil degradation and crop toxicity[7,8]; however, conventional remediation approaches (e.g., membrane filtration[9] and phytoremediation[10] remain constrained by high energy demands or spatial limitations.

While adsorption[11]and bioremediation[12] demonstrate technological potential, their scalability limitations hinder large-volume drainage water treatment applications, prompting the need for alternative solutions. Soil Aquifer Treatment (SAT) has emerged as a viable approach that leverages natural soil filtration processes for pollutant removal through controlled infiltration[13]with well-documented efficacy in organic carbon degradation[14]nutrient retention[15]and pathogen reduction[16]. However, critical knowledge gaps persist, particularly regarding salt accumulation dynamics, as existing studies[17–20] lack mechanistic insights into depth-specific salt migration under variable salinity loads, which may lead to long-term soil clogging. Furthermore, the absence of established thresholds for safe inflow concentrations (e.g., salinity, TDS) impedes the integration of SAT with agricultural irrigation standards[4]highlighting the need for further research to optimize system design and operational parameters.

While computational modeling tools such as Hydrus-1D[21–24]and SWAP[25] demonstrate capability in simulating water-solute transport dynamics, they exhibit two significant limitations that warrant consideration. First, current modeling approaches inadequately represent layer-specific salt retention mechanisms in stratified soil profiles, particularly under conditions of groundwater table fluctuation[19]. Second, the absence of a

[1]Engineering Research Center of Agricultural Microbiology Technology, Ministry of Education, Heilongjiang University, Harbin 150500, China. [2]Institute of Water Conservancy and Electric Power, Heilongjiang University, Harbin 150080, China. ✉email: 2020023@hlju.edu.cn

standardized framework for correlating simulated transport parameters with established irrigation water quality benchmarks presents a substantial methodological gap in operational applications.

This study integrates laboratory soil column experiments with Hydrus modeling to investigate a rice irrigation district in Wuhan, China, with dual objectives: (1). elucidate infiltration patterns and hydro-saline transport mechanisms of agricultural drainage with varying salinity levels through SAT systems, quantifying depth-specific salt accumulation dynamics; (2) develop a mathematical model establishing maximum permissible inflow concentrations based on irrigation water quality standards, providing theoretical guidance for optimized SAT system operation.

Research methods
Water sample collection
The research specimens were obtained from paddy fields in Huangpi District, Wuhan City, Hubei Province (30°52'N, 114°23'E), with sampling conducted on August 2, 2023 – a critical late-growth phase of rice cultivation characterized by field drainage and sunning practices. This temporal selection ensures representative sampling of agricultural drainage water under typical farming operations. Field collection strictly adhered to the Technical Specifications for Environmental Quality Monitoring of Agricultural Water Sources (NY/T 396–2000).

One-dimensional soil column infiltration experiments
To address the challenges of field heterogeneity in hydrogeological studies, a controlled soil column system was developed to simulate natural percolation dynamics. The apparatus comprised a transparent polymethyl methacrylate (PMMA) column (60 cm height × 10 cm inner diameter) with an effective infiltration length of 45 cm, coupled with a Mariotte bottle (6 cm inner diameter × 20 cm height) to maintain a constant hydraulic head[26]. The soil column was instrumented with a vertically distributed sensor array along a defined coordinate system (X = 0 at 45 cm depth from column base, positive downward). Three horizontally aligned access ports were established at each of four strategic depths: 7 cm, 19 cm, 31 cm, and 43 cm from the column top. Each port accommodates a sensor for simultaneous measurements of volumetric water content (θ) and electrical conductivity (EC) at 1-minute intervals. A 60-cm flexible ruler affixed along the column exterior facilitated manual tracking of wetting front progression through transparent polycarbonate walls.

Quartz sand was selected as the infiltration medium in this study due to its uniform particle morphology, controllable particle size distribution, and chemical inertness. As the primary component of quartz sand is SiO_2, it exhibits negligible chemical interactions with dissolved salts (e.g., Na^+, Cl^-), effectively eliminating interference from chemical adsorption or precipitation during water-salt transport processes. This inertness ensures that observed dynamics exclusively reflect physical transport mechanisms rather than chemical transformations[27]. Artificial recharge water was prepared using sodium chloride (NaCl) solutions to simulate brackish irrigation conditions. The detailed schematic diagrams of the experimental apparatus are systematically depicted in Fig. 1.

Three quartz sand fractions with distinct particle size ranges were selected for the experimental configurations: fine sand(0.13–0.18 mm), medium sand(0.25–0.45 mm), coarse sand(0.85–2.0 mm). Four soil column configurations (G1–G4) were constructed by stratifying these sand fractions, with layer-specific physical properties summarized in Table 1.
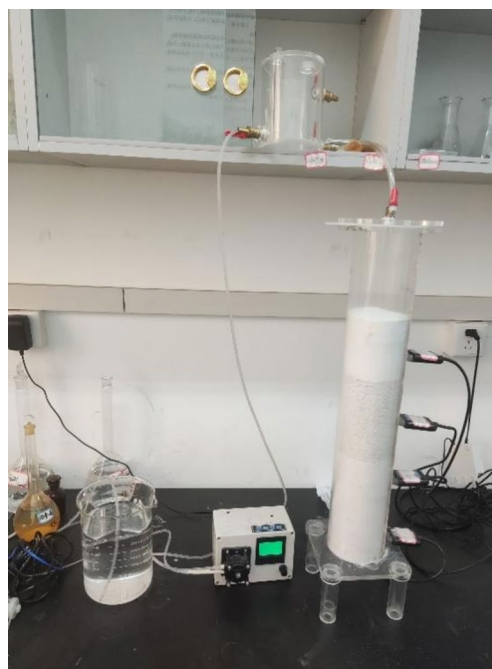

Fig. 1. Physical diagram of experimental device.

$$y = EC * 3.77 - 0.24 \tag{1}$$

where calibration coefficients were derived from standardized NaCl reference solutions. This systematic approach enabled precise characterization of water-salt transport mechanisms under controlled yet environmentally representative conditions.

Where y = soil salt content (total dissolved solids, g/L).

EC = soil electrical conductivity (mS/cm, standardized to 25 °C).

Hydrus simulation

Hydrus mathematical model

Given the predominantly vertical infiltration patterns observed in the experimental soil column, the system was conceptualized as a 1D vertical transport model. The water movement is governed by the Richards equation:

$$\frac{\partial \theta}{\partial t} = \frac{\partial}{\partial z}\left[k(h)\left(\frac{\partial h}{\partial z} + 1\right)\right] \tag{2}$$

Where: t——time(d);

θ——soil volumetric water content(cm³/cm³);

h——pressure head(cm);

z——vertical space coordinate(cm);

k(h)——unsaturated hydraulic conductivity(cm/d).

Soil salt transport is described by a one-dimensional convective one-dispersion equation:

$$\frac{\partial(\theta C)}{\partial t} = \frac{\partial}{\partial z}\left(D_{ij}\frac{\partial C}{\partial z}\right) - \frac{\partial(q_i\theta)}{\partial z} \tag{3}$$

Where: C——solute mass salt content (g/100 g),

D_{ij}——dispersion coefficient (cm²/h),

q_i—— volumetric flux (cm/h).

Hydrus initial and boundary conditions

The initial soil moisture conditions are determined from the soil moisture profile measured at the beginning of the simulation, and the initial conditions for soil moisture transport can be expressed as follows:

$$\theta(z, t = 0) = \theta_0(z) \{\ 0 \leq z \leq Z \tag{4}$$

Where: $\theta_0(z)$—— initial soil water content (cm³/cm³),

Z—— maximum vertical distances (cm)of the simulation calculation area, respectively.

In this study, the one-dimensional simulation of the soil columns was performed only for the vertical distances, Z = 45 cm.

The water flow model for simulating the soil profile incorporates the following boundary conditions:

Soil layer structure	Depth of soil layer/cm	Particle size/mm	Bulk density of soil/g.cm⁻³
G1	0–45	0.25–0.45	1.58
G2	0–10	0.13–0.18	1.62
	11–25	0.25–0.45	1.58
	26–45	0.85-2	1.44
G3	0–20	0.85-2	1.44
	21–35	0.25–0.45	1.58
	36–45	0.13–0.18	1.62
G4	0–10	0.13–0.18	1.62
	11–30	0.85-2	1.44
	31–45	0.25–0.45	1.58

Table 1. Basic properties of soil samples of each layer. Soil packing followed standardized protocols, with stratified installation at controlled bulk density (5 cm/layer) and interfacial scarification to ensure hydraulic continuity. This protocol achieved a homogeneous 45 cm soil profile representative of typical Soil Aquifer Treatment (SAT) vadose zone conditions. During infiltration, wetting front progression and hydraulic head variations were continuously recorded. Following the completion of infiltration, depth-specific soil moisture content and salinity levels were systematically recorded. Volumetric water content (θ) was measured in situ using sensors installed at each monitoring depth (7 cm, 19 cm, 31 cm, and 43 cm). Simultaneously, soil electrical conductivity (EC) was quantified via integrated conductivity probes, with measurements automatically logged at 1-minute intervals. To enhance simulation fidelity in HYDRUS-1D, the measured electrical conductivity (EC) values were systematically converted to total dissolved solids (TDS) concentrations using the experimentally derived linear calibration relationship:.

Upper boundary: constant pressure head

$$h_{(x,y,z,t)} = h_i \qquad (5)$$

Lower boundary: free drainage

$$h_{(z,t)} = h_0 \qquad (6)$$

Where: x,y, z—— spatial coordinate (cm),
    t—— time(h),
    h_i—— water depth (cm),
    h_0—— the initial matric head distribution within the soil profile (cm).
    In this study, soluble salts were selected as the research subject to investigate solute transport dynamics. The upper boundary was assigned a concentration flux boundary condition with deionized irrigation water, while the lower boundary adopted a zero concentration gradient boundary condition. The initial conditions were defined as the volumetric water content (θ) of each individual soil layer.
    Initial condition:

$$c\left(z,0\right) = c_0\left(z\right) = 0 \quad 0 \le z \le Z \qquad (7)$$

Upper boundary: concentration flux boundary

$$\left[D\frac{\partial c}{\partial z} + \epsilon_i\right]_{iz} = 0 \qquad (8)$$

Lower Boundary: zero concentration

$$c(z,t)_{iz=z} = c_0 \qquad (9)$$

Where: c—— solute mass salt content (g/100 g),
    c_0——initial salt content of each layer of soil (g/100 g),
    ϵ_i—— evaporation intensity (cm/h).
    Z—— maximum vertical distance in the simulated region (cm).

Model parameters and input data
Soil water movement parameters include saturated hydraulic conductivity K_S, saturated water content θs, residual water content θr, and fitting parameters α,n. Solute transport parameters include soil density (ρ) and dispersivity(DLetc). The soil hydraulic properties were determined using the Van Genuchten (VG) model for soil water retention characteristics. The required VG parameters (α,n, θs, and θr) were inversely estimated through the Rosetta module integrated within the HYDRUS software environment. For solute transport parameters, we employed an inverse modeling approach based on experimental data obtained from laboratory soil column experiments.
    The specific parameters are shown in Table 2:

Conclusions of the experiment
Analysis of water samples
Water samples collected from the rice paddy fields in Wuhan underwent comprehensive analysis following the Agricultural Irrigation Water Quality Standards (GB 5084 – 2021). As summarized in Table 3, all evaluated parameters met or significantly outperformed the regulatory thresholds for Class I irrigation water, confirming the suitability of the water source for agricultural reuse.
    9 types of water chemical characterization were carried out on the collected farmland drainage water samples, in which all 6 basic control items of the water samples met the standards, the PH value as well as the concentration of conventional ions met the standards, and the 3 selective control items also basically complied

Soil column structure	G4		
Depth of soil(cm)	0–10	11–30	30–45
Soil type	Fine sand	Coarse sand	Medium sand
ρ(g/cm³)	1.62	1.44	1.58
θs(cm³/cm³)	0.38	0.436	0.43
θr(cm³/cm³)	0.047	0.040	0.045
α	0.0412	0.13	0.015
n	2.21	2.65	2.68
K_S(cm/min)	0.2	0.495	0.4
Dispersivity (cm)	0.5	0.203	0.24

Table 2. The parameters of soil-water movement and solute transport.

	Program	Test result	Standard	Qualified or not
Basic control item	pH	7.74	5.5< pH<8.5	Yes
	Cl⁻	36.88 mg/L	<350 mg/L	Yes
	Pb	<0.002 mg/L	0.05 mg/L	Yes
	Cr	<0.004 mg/L	≤0.1 mg/L	Yes
	Cd	<0.0005 mg/L	≤0.01 mg/L	Yes
	Hg	0.00015 mg/L	≤0.001 mg/L	Yes
Selective control item	Cu	<0.02 mg/L	0.5 mg/L	Yes
	Zn	<0.03 mg/L	1 mg/L	Yes
	Se	<0.001 mg/L	0.02 mg/L	Yes

Table 3. Comparison of agricultural drainage water quality with standards.

with the requirements. The pH value in the normal range indicates the acid-base balance of the water body, which is conducive to the survival of aquatic organisms and the stability of the water body ecosystem. The content of heavy metal elements such as mercury, cadmium, and lead is extremely low, all below the very low limit stipulated in"Agricultural Irrigation Water Quality Standard "(GB 5084−2021). For example, the mercury level of 0.00015 mg/L is well below 0.001 mg/L. This indicates that there is no risk of heavy metal contamination in agricultural drainage. However, the presence of Cl-in the water can also be seen in the water sample test results. Continued infiltration of low levels of chloride ions in the water may have multiple potential impacts on the SAT system, ultimately affecting the effectiveness of the SAT system for water quality purification. Therefore, monitoring of chloride infiltration is required in the operation and management of SAT systems.

Impact of different grades on the infiltration of brackish water

Infiltration experiments were conducted using 2.5 g/L NaCl solution in repacked soil columns to examine how textural gradation influences coupled water and solute transport dynamics.

Migration law of wetting fronts under different gradations
The temporal evolution of wetting front progression under brackish water infiltration across different soil textures is illustrated in Fig. 2. The y-axis is depth below column top (0 cm = inlet) and the column bottom position (45 cm). Total infiltration durations followed the order: G2 (170 min) > G4 > G1 > G3 (98 min), indicating distinct permeability characteristics among soil configurations. Based on the experimental measurements, we observed a 73.4% enhancement in infiltration rate for configuration G3 compared to G2 (the slowest-performing case). This significant difference demonstrates the critical impact of textural gradation on hydraulic efficiency[28]. Analysis of upper-layer wetting front migration revealed a hierarchical relationship: coarse sand infiltration time < medium sand < fine sand. This pattern aligns with established hydraulic conductivity principles reported in analogous soil-water systems[29]. The textural composition of soil exerts a significant influence on its hydraulic conductivity and infiltration capacity[30].

The infiltration process exhibited distinct phase-dependent variations across soil configurations, revealing critical impacts of layered textural structures on moisture movement. Initial infiltration rates demonstrated marked differences, with G3 showing significantly higher velocity compared to other groups (G2 and G4 exhibited comparable rates, both lower than G1). However, during secondary layer penetration, G3's migration velocity decelerated, while G4's wetting front accelerated. Notably, G2 displayed the highest terminal velocity in the basal layer. This nonlinear progression underscores the capillary barrier effects at soil layer interfaces[31]. Analysis of adjacent-layer wetting front dynamics revealed transient stagnation at textural transitions (e.g., from Grading 1 to Grading 2), attributed to heterogeneous capillary distributions at interfaces[32]which induce abrupt hydraulic potential shifts and impede infiltration—termed the "water-blocking effect." Full penetration into subsequent layers occurs only when the upper layer's negative pressure head exceeds the air-entry suction of the underlying coarser stratum. Coarser, more uniform lower layers intensify this capillary barrier effect[33]with greater textural contrast between layers amplifying the water-blocking efficacy[34]. These findings systematically elucidate how stratified soil architectures modulate infiltration patterns through coupled capillary and textural interactions.

Changes in soil water content under different gradations
Figure 3 depicts the variation of soil water content with depth in different soil grades. It can be seen that the initial volumetric water content of each layer of homogeneous soil (G1) is basically equal, with an average value of 4.2%, but in the stratified soils (G2, G3, G4), the initial water content is not the same, because of the water-holding capacity of the soils in different grades is different.It can be seen that the larger the grain size of the soil, the lower the initial water content. The trend of water content with time is basically similar to that of the wetting front. When the wetting front arrived, the water content of the soil layer increased rapidly and gradually increased to the maximum water content of the soil over time. The overall trend of the water content of the four soil columns is consistent.

Figure 3 delineates the vertical distribution of volumetric water content (θ) across soil profiles with varying textural configurations. In homogeneous soil (G1), the initial θ values exhibited uniform layering, averaging 4.2% throughout the profile, consistent with its isotropic structure. Conversely, stratified soils (G2, G3, G4)
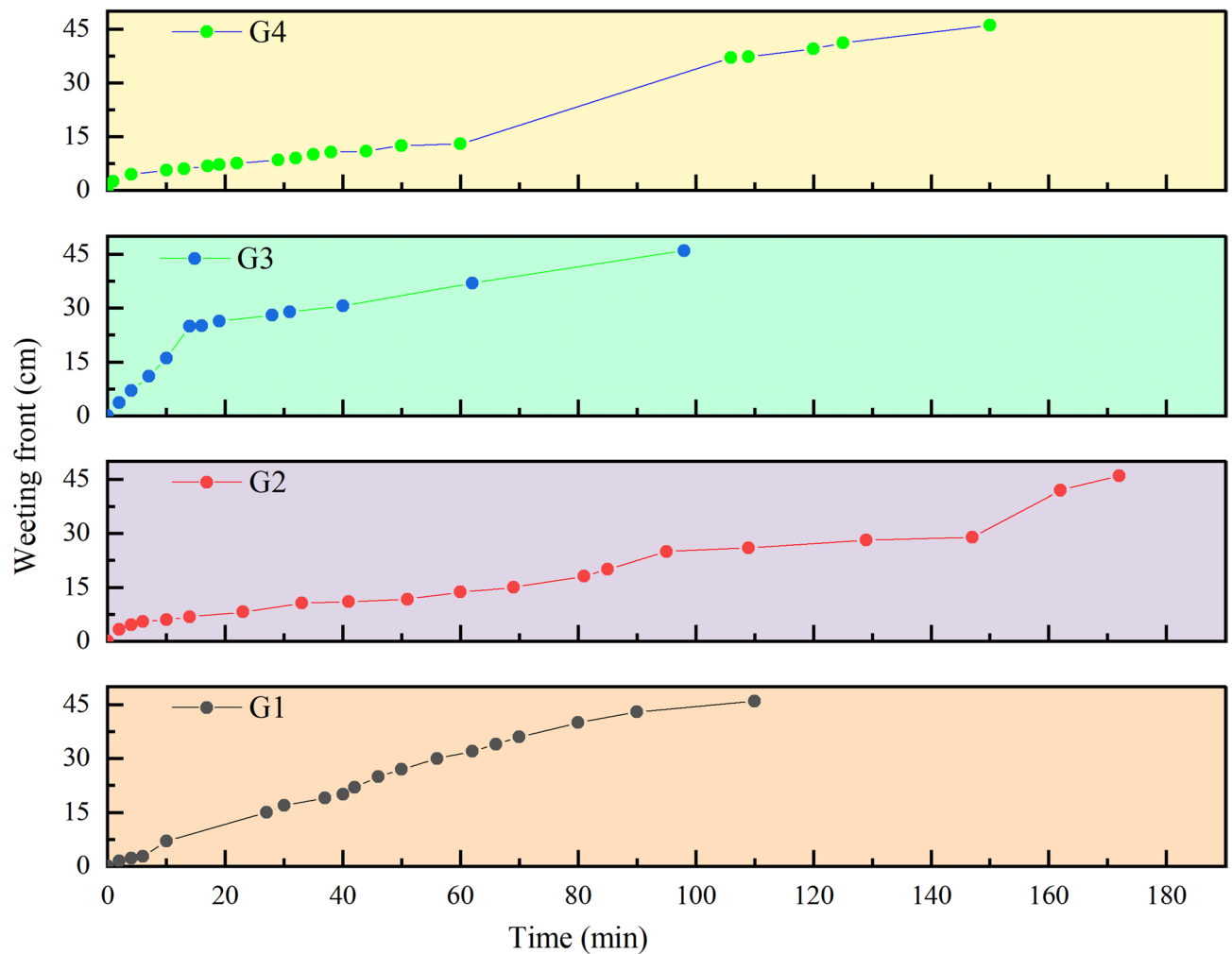
Fig. 2. Divergent wetting front trajectories reflect texture-dependent hydraulic properties.
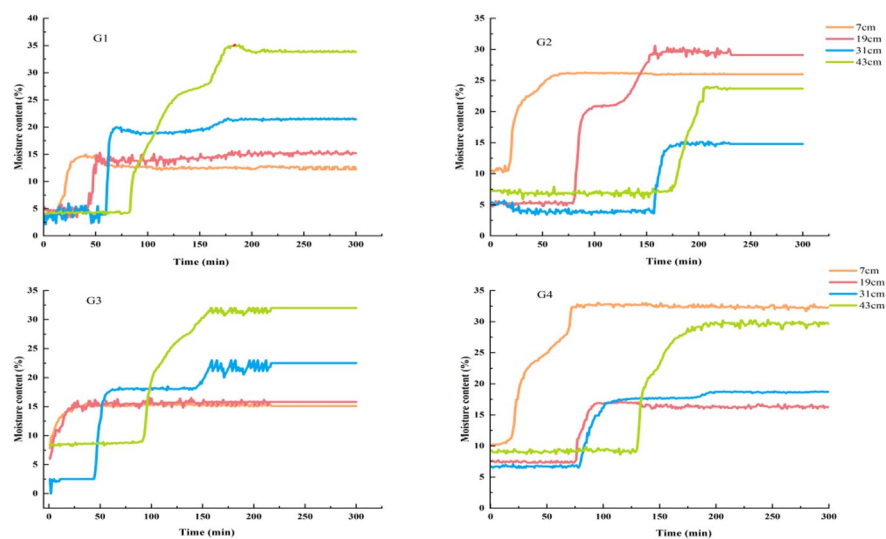

Fig. 3. The moisture content of unsaturated soil varies with time under the four structures.

displayed texturally dependent heterogeneity in initial θ, reflecting differential water retention capacities across soil gradations. Notably, coarser-textured layers demonstrated lower initial θcompared to finer-textured strata, validating the inverse correlation between soil particle size and water retention capacity. The temporal variation of volumetric water content closely mirrored the progression pattern of the wetting front. Upon the arrival of the wetting front at a given soil layer, the water content exhibited a rapid increase, gradually approaching the soil's maximum water-holding capacity over time. All four soil columns demonstrated consistent temporal patterns in water content evolution.

Horizontal comparison of surface layers across the four configurations revealed consistently higher volumetric water content in fine sand layers, attributed to their smaller particle size and superior water retention capacity. Under equivalent conditions, reduced particle size correlates with increased water content. Vertical comparison between fine sand layers in G2 and G3 demonstrated elevated water content in G3 versus G2 despite identical textural classification. This discrepancy arises from gravity-driven infiltration dynamics: during percolation, rapid drainage from upper layer pores (high hydraulic conductivity) leads to initial moisture depletion, while continuous water accumulation in lower strata (low hydraulic conductivity) progressively elevates their water content and electrical conductivity[35].

Changes in soil conductivity under different grades
Electrical conductivity (EC) provides an efficient indirect measure of soil salinity, strongly correlating with salt content. As shown in Fig. 4, sustained brackish water infiltration induced progressive salt accumulation across soil layers, with salt leaching depth—the maximum vertical extent of effective salt removal—varying significantly by soil configuration. Homogeneous coarse-textured soils (G1, G3) achieved deeper leaching depths (≥ 19 cm) due to high hydraulic conductivity whereas heterogeneous layered systems (G2, G4) exhibited shallow leaching (< 7 cm) owing to capillary barrier effects at textural interfaces. These results highlight that soil architecture critically governs salt redistribution: coarse textures enhance vertical flushing, while abrupt particle size contrasts trap salts in upper layers. Optimizing graded soil sequences and monitoring EC thresholds are thus essential for improving SAT-mediated salinity management in agricultural drainage systems.

Analysis of electrical conductivity (EC) across soil layers in the four column configurations revealed distinct salt retention capacities influenced by soil texture and stratification. The efficacy of salt retention followed the hierarchy: fine sand > medium sand > coarse sand, indicating that particle size governs both hydrological dynamics and solute distribution. This trend highlights the superior salt-blocking capacity of interlayered configurations (e.g., G4: fine-coarse-medium) compared to homogeneous soils (G1). Textural stratification within soil columns significantly impedes vertical salt migration, effectively reducing salt accumulation in deeper soil layers. Comparative analysis of overall salt retention efficacy across column configurations revealed the hierarchy: G4 > G2 > G3 > G1. The fine-coarse-medium stratified structure (G4) demonstrated optimal salt retention performance.

Analysis of the electrical conductivity (EC) trends in the four soil columns reveals that soil salt migration follows water movement, with solute dispersion occurring in the loamy soil. During infiltration, the EC values in each soil layer from top to bottom initially increased sharply and then stabilized. Unlike conventional solute migration dominated by adsorption-desorption equilibria, soil salt transport follows a "salt-water coupling" mechanism.

Effects of infiltration of different concentrations of brackish water on soil
The G4 configuration, identified as the optimal salt barrier structure, was selected for subsequent investigation of salinity transport dynamics under varying influent mineralization levels. Controlled infiltration experiments
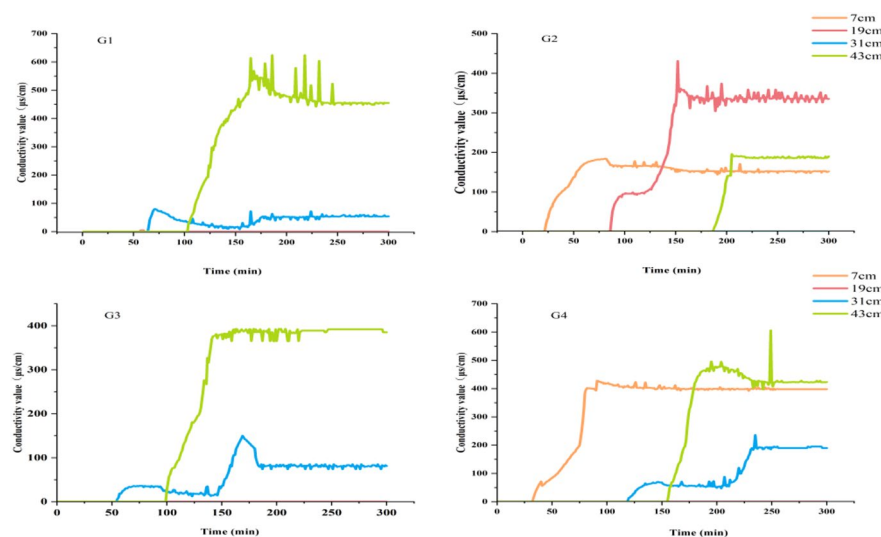

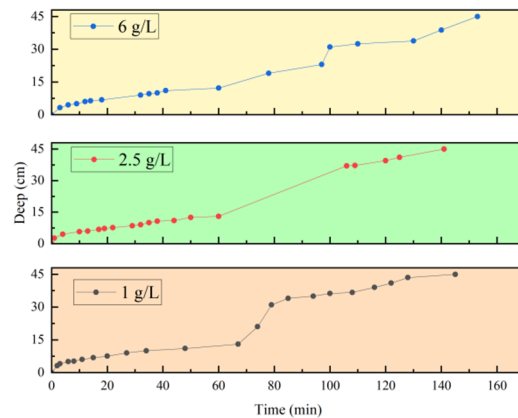**Fig. 4**. The conductivity of unsaturated soil varies with time under four kinds of structures.

Fig. 5. Variation of wetting front with time under three mineralization levels.
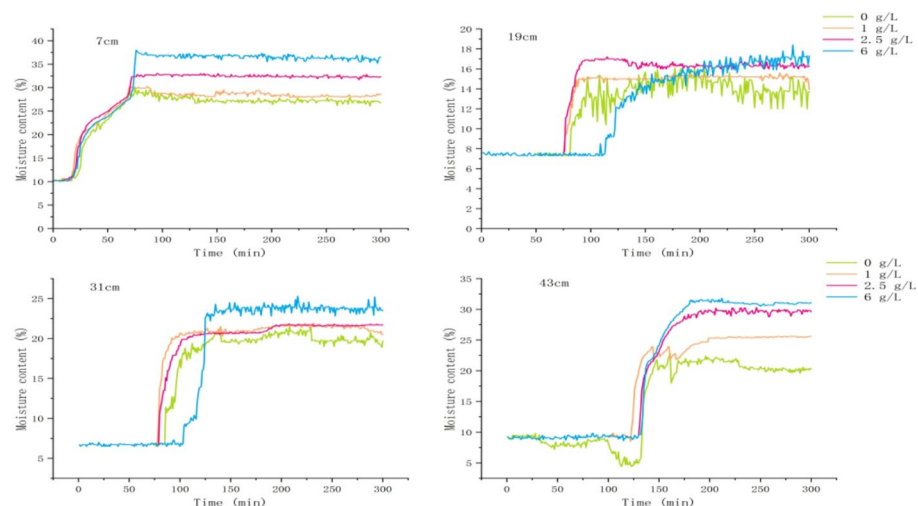

Fig. 6. Change of soil moisture content under infiltration of three kinds of salinity.

were conducted using brackish water with three distinct mineralization gradients (1, 2.5, and 6 g/L), maintained under constant hydraulic head conditions.

Characteristics of wetting front changes
Experimentally determined wetting front migration for the three mineralizations is shown in Fig. 5:

As shown in Fig. 5, the movement of the wetting front under the three mineralization levels (1, 2.5, and 6 g/L) followed similar trends. The wetting front moved slowest between 0 and 11 cm, fastest between 11 and 31 cm, and moderately between 31 and 46 cm. These rates matched the soil layer structure: coarse sand > medium sand > fine sand, meaning water infiltrated faster in coarser layers. At the start of infiltration, all treatments showed relatively high soil infiltration rates. As infiltration continued, the rates gradually decreased and stabilized over time.

Analysis of infiltration rates across different salinity levels revealed the following hierarchy: 2.5 g/L > 1 g/L > 6 g/L.When the mineralization level of infiltrating water increased from 1 to 2.5 g/L, elevated ionic concentrations enhanced interparticle interactions within the soil column, promoting a more compact and ordered structure. This structural optimization improved hydraulic conductivity by creating more permeable pathways for water infiltration[27,36]. However, at a mineralization level of 6 g/L, excessive ionic concentrations induced pronounced gelation effects, which over-consolidated the soil matrix. The resultant reduction in interparticle porosity significantly impeded water infiltration dynamics[37].

Changes in soil water content and electrical conductivity at different levels of mineralization
When infiltration was carried out using brackish water with different levels of mineralization, the changes in moisture content of the soil layers are shown in Fig. 6:

As demonstrated in Fig. 6, the temporal-spatial variations in soil water content across column layers align with the inherent physicochemical properties of the soil textures. Specifically, salinity elevation significantly enhanced the water content across all soil layers. This phenomenon arises because Na⁺ and Cl⁻ ions in high-
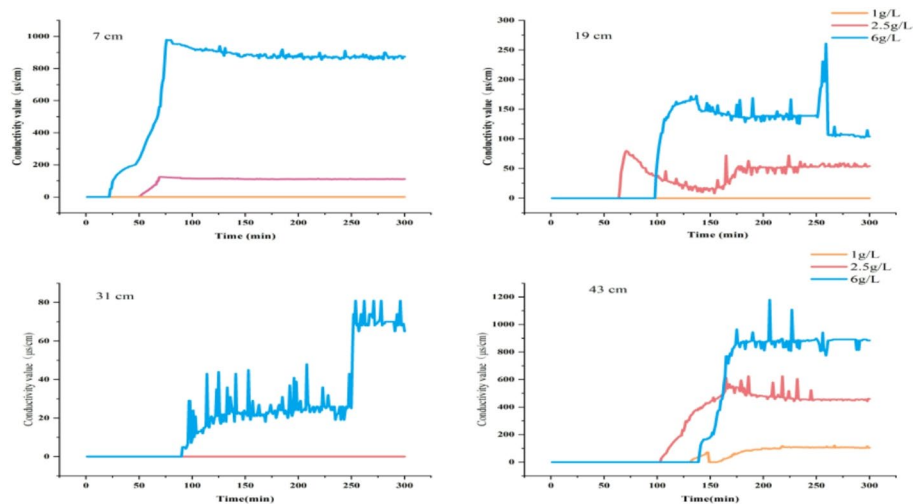
Fig. 7. Change of conductivity with time under three kinds of mineralization.
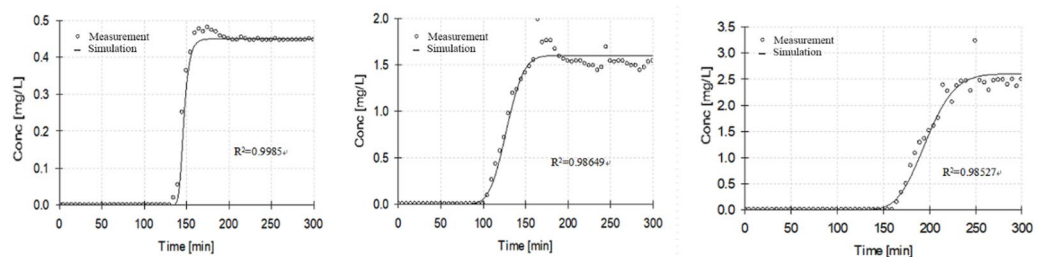

Fig. 8. Data simulation results under three kinds of mineralization.

salinity solutions carry associated hydration shells (with a typical single-ion hydration shell thickness of approximately 0.3–0.8 nm), substantially increasing the bound water content within micropores. Concurrently, the fine sand layer exhibits greater sensitivity to salinity in terms of water retention capacity, attributable to its high specific surface area, which strengthens water-ion interactions. Conversely, the large pores in the coarse sand layer are dominated by free water, resulting in a weaker bound water effect.

Water conductivity, measured in microsiemens per centimeter (μS/cm), is directly related to salinity, which is the concentration of dissolved salts in water. As shown in Fig. 7, when salts, such as sodium chloride (NaCl), dissolve in water, they dissociate into ions (Na^+ and Cl-), increasing water's ability to conduct electricity. Dissociated salts increase the number of free ions in water, which elevates conductivity. The higher the concentration of salts, the higher the conductivity.

SAT site operation simulation

Calibration and validation of the hydrus model

Data at 7 cm during infiltration of brackish water of the three mineralizations into the fine-medium-coarse soil column during the experimental period were selected, and the measured and simulated values were compared to verify the accuracy of the model, as shown in Fig. 8:

The figure demonstrates that the model achieves an $R^2 > 0.98$, indicating excellent accuracy with close agreement between simulated and measured values.

SAT site simulation

Based on the research team's prior findings[38] which indicate that rice paddies require 3–5 drainage events during the growth cycle, with each event lasting ≤ 12 h, the operational duration of the Soil Aquifer Treatment (SAT) site was established at 60 h to accommodate cumulative drainage needs. To define the permissible salinity threshold for SAT optimization, the *Agricultural Irrigation Water Quality Standard* (GB 5084 − 2021) was referenced, setting the maximum allowable salinity concentration for farmland irrigation in Wuhan at 1 g/L. Consequently, the simulated infiltration concentrations were parameterized within the range of 0.7–1.9 g/L to evaluate system performance under near-threshold conditions.

Experimental results demonstrated that the fine-coarse layered soil structure exhibited the highest salt retention efficacy. Consequently, this study focuses on simulating the hydro-saline dynamics of fine-coarse
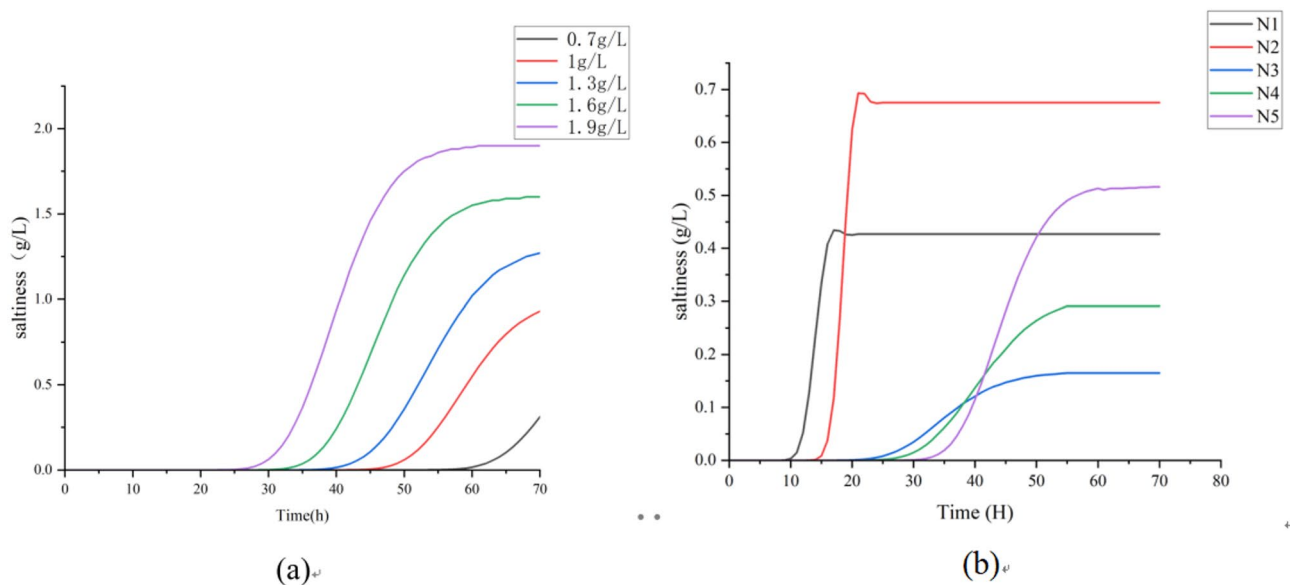
Fig. 9. (a) SAT field operation simulation results, (b) SAT site salt distribution simulation results.

stratified soil columns to optimize SAT performance under brackish irrigation. The simulation results are shown below:

As demonstrated in Fig. 9a, the infiltration rate exhibits a concentration-dependent acceleration within the tested range of 0.7–1.9 g/L, consistent with experimental observations. At a critical infiltration concentration of 1.3 g/L, the system achieves equilibrium between influent salinity and effluent threshold limits (1 g/L as per GB 5084 – 2021) precisely at the 60-hour operational timeframe. This inflection point signifies the maximum permissible infiltration concentration for SAT systems under the specified hydraulic and textural conditions, beyond which effluent salinity exceeds regulatory standards.

To monitor salt transport dynamics, five observation points were established at key interfaces: mid-fine sand (N1), fine sand base (N2), mid-coarse sand (N3), coarse sand base (N4), and mid-medium sand (N5). Meanwhile, the curve corresponds to a depth of 1.8 m. Simulation results (Fig. 9b) align with experimental findings, confirming that fine sand exhibits the highest salt retention capacity, followed by medium and coarse sands. The maximum salt accumulation (0.0675 g/L) occurred at the fine sand base (N2), where the significant textural contrast between fine and coarse layers prolonged brackish water retention. This extended contact time enhanced ionic adsorption and capillary retention, demonstrating that interfacial gradation differences critically govern salt redistribution efficiency.

According to Sun Xing[39] salt content promotes soil N_2O emission when the salt content ranges from 0 to 17 g/L; according to CHEN[40] if the salinity is less than 1 g/L, the diversity of microorganisms, although affected, is small7. Therefore, when 1.3 g/L brackish water was infiltrated, the maximum salt content of the soil layer in the SAT system was 0.7 g/L, which was less than 1 g/L, and had little effect on microbial activity and could promote soil N_2O discharge. Overall, 1.3 g/L of brackish water as a critical value for infiltration into the SAT system meets the criteria for agricultural water recharge and does not impact the operation of the site, which can be guaranteed.

Conclusion

This study, through controlled indoor simulation experiments, revealed that soil structural heterogeneity significantly influences brackish water infiltration dynamics. In homogeneous soils, wetting front progression maintained constant velocities, whereas layered soil configurations exhibited variable infiltration rates modulated by textural gradation variations. Specifically, layered architectures enhanced cumulative water infiltration volumes compared to homogeneous counterparts. The water retention and salt barrier efficacy followed a hierarchical pattern: fine sand > medium sand > coarse sand, with the fine-medium-coarse stratified structure demonstrating optimal salt retention performance under equivalent experimental conditions. These findings quantitatively establish textural sequencing as a critical determinant of vadose zone hydrological behavior in saline irrigation contexts.

Saline water irrigation elevates soil moisture content while concurrently increasing soil salinity, demonstrating a direct positive correlation between influent salinity and resultant soil salinity levels. Mineralization exerts a concentration-dependent influence on soil infiltration performance: within the range of 1–2.5 g/L, elevated mineralization enhances infiltration efficiency through improved soil structure stability and pore connectivity. However, beyond 2.5 g/L(up to 6 g/L), infiltration efficiency declines progressively with increasing mineralization, attributable to excessive ionic strength effects that disrupt soil colloid stability and reduce effective porosity. Among the three tested brackish waters with distinct salinities, water containing 2.5 g/L exhibited characteristic threshold behavior. However, due to an inadequate number of samples in this study, experiments were not

conducted using saline waters within the 2.5 g/L to 6 g/L salinity range. Consequently, the specific threshold within this interval could not be confirmed. Future comprehensive investigations addressing this salinity gradient are required.

Building upon these efforts, we developed a numerical model that effectively simulates water-salt transport dynamics at the SAT site. The simulated values demonstrate strong agreement with measured data ($R^2 > 0.98$), validating the model's predictive reliability. Simulation results indicate that under the fine-coarse-medium sand layering configuration, the influent concentration should be maintained below 1.3 g/L to ensure peak soil salinity remains ≤ 0.675 g/L—a threshold compatible with sustained SAT system functionality. Exceeding this concentration necessitates pretreatment (e.g., reverse osmosis or dilution) to mitigate salinity accumulation risks and maintain operational stability.

Data availability

Some or all data that support the findings of this study are available from the corresponding author upon reasonable request.

References

1. Sang, Z. et al. Effective solutions to ecological and water environment problems in the Sanjiang plain: utilization of farmland drainage resources. *Sustainability*, **15**(23), (2023).
2. Wang, Z. H. et al. Spatial and Temporal matching characteristics and influencing factors of agricultural water and soil resources in China [J]. *People Yangtze River*. **55**, 116–124. https://doi.org/10.16232/j.cnki.1001-4179.2024.02.015 (2024).
3. Zahran, M. N. H. Assessment of agricultural drainage water quality for safe reuse in irrigation applications-a case study in Borg El-Arab, Alexandria. *J. Coastal. Life Med.* https://doi.org/10.12980/jclm.3.2015j5-4 (2015).
4. Pedrero, F., Kalavrouziotis, I., Alarcón, J. J., Koukoulakis, P. & Asano, T. Use of treated municipal wastewater in irrigated agriculture—Review of some practices in Spain and Greece. *Agric. Water Manage.* **97**, 1233–1241. https://doi.org/10.1016/j.agwat.2010.03.003 (2010).
5. Wei, H. B., Wang, Y., Liu, J. & Zeng, R. Heavy metal in river sediments of Huanghua City in water diversion area from yellow river, china: contamination, ecological risks, and sources. *WATER* **15** https://doi.org/10.3390/w15010058 (2023).
6. Wang, S. L., Xu, D., Fang, S. X., Wu, C. L. & Yang, J. G. Water quality risk assessment of farmland drainage reuse in Yinbei irrigation district, Ningxia[J]. *Agricultural Res. Dry. Areas.* **28**, 43–47 (2010).
7. Chen, X. M., Wo, F., Chen, C. & Fang, K. Seasonal changes in the concentrations of nitrogen and phosphorus in farmland drainage and groundwater of the Taihu lake region of China. *Environ. Monit. Assess.* **169**, 159–168. https://doi.org/10.1007/s10661-009-1159-3 (2010).
8. Mainardis, M. et al. Wastewater fertigation in agriculture: issues and opportunities for improved water management and circular economy. *Environ. Pollut.* **296**, 118755. https://doi.org/10.1016/j.envpol.2021.118755 (2022).
9. Wu, J., Zhang, Y. Y., Wang, J., Zheng, X. & Chen, Y. G. Municipal wastewater reclamation and reuse using membrane-based technologies: a review. *Desalination Water Treat.* **224**, 65–82. https://doi.org/10.5004/dwt.2021.27175 (2021).
10. Li, Y. Y., Shao, X. H. & Sheng, Z. P. Field experiments on reducing pollutants in Agricultural-Drained water using Soil-Vegetation buffer strips. *Pol. J. Environ. Stud.* **25**, 195–204. https://doi.org/10.15244/pjoes/60897 (2016).
11. Li, J., Wang, H. Y., Wang, Y., Ma, M. Z. & Ma, J. Y. Selection test of filter material for farm drainage dark pipe based on regression water reuse . *Water-saving Irrigation*. 18–25 (2022). (In Chinese)
12. Mora-Ravelo, S. G., Alarcón, A., Rocandio-Rodríguez, M., Vanoye-Eligio, V. & BIOREMEDIATION OF WASTEWATER FOR REUTILIZATION IN AGRICULTURAL SYSTEMS. A REVIEW. *Appl. Ecol. Environ. Res.* **15**, 33–50. https://doi.org/10.15666/aeer/1501_033050 (2017).
13. Zhang, G., Zhu, J., Yang, K., Zhu, Y. & Sang, Z. Design of an enhanced SAT using zeolite for the removal of ammonia nitrogen at a Bengbu aquatic farm in China. *Sustainability.* **14**(24), (2022).
14. Zhang, X., Zhao, X., Gao, Y. T. & Zhang, M. Removal of effluent dissolved organic matter of different molecular sizes by advanced treatments and soil infiltration. *Water Environ. Res.* **86**, 81–86. https://doi.org/10.2175/106143013X13807328848856 (2014).
15. Abel, C. D. T., Sharma, S. K., Mersha, S. A. & Kennedy, M. D. Influence of intermittent infiltration of primary effluent on removal of suspended solids, bulk organic matter, nitrogen and pathogens indicators in a simulated managed aquifer recharge system. *Ecol. Eng.* **64**, 100–107. https://doi.org/10.1016/j.ecoleng.2013.12.045 (2014).
16. Sanz, C. et al. Efficient removal of toxicity associated to wastewater treatment plant effluents by enhanced soil aquifer treatment. *J. Hazard. Mater.* **465**, 133377. https://doi.org/10.1016/j.jhazmat.2023.133377 (2024).
17. Zhu, J., Pei, Q. Q., Guo, Q. L. & Zhang B. Study on distribution characteristics of water and salt transport in rammed soil based on size effect [J]. *Rock. Soil. Mech.* **45**, 1481–1494. https://doi.org/10.16285/j.rsm.2023.0928 (2024).
18. Wang, Z. M., Jin, M. G., Simunek, J. & van Genuchten, M. T. Evaluation of mulched drip irrigation for cotton in arid Northwest China. *Irrig. Sci.* **32**, 15–27. https://doi.org/10.1007/s00271-013-0409-x (2014).
19. Nie, S. Y., Bian, J. M. & Zhou, Y. C. Estimating the Spatial distribution of soil salinity with geographically weighted regression kriging and its relationship to groundwater in the Western Jilin irrigation area, Northeast China. *Pol. J. Environ. Stud.* **30**, 283–293. https://doi.org/10.15244/pjoes/121988 (2021).
20. Chen, W. et al. Corrigendum to 'Spatial distribution of soil moisture, soil salinity, and root density beneath a cotton field under mulched drip irrigation with brackish and fresh water' [Field Crops Research 215 207–221]. *Field Crops Research* **226**, 83, (2018). https://doi.org/10.1016/j.fcr.2018.08.004 (2018).
21. Ebrahimian, H., Liaghat, A., Parsinejad, M., Abbasi, F. & Navabian, M. Comparison of One- and Two-Dimensional models to simulate alternate and conventional furrow fertigation. *J. Irrig. Drain. Eng.* **138**, 929–938. https://doi.org/10.1061/(ASCE)IR.1943-4774.0000482 (2012).
22. Simunek, J., van Genuchten, M. T. & Sejna, M. Development and applications of the HYDRUS and STANMOD software packages and related codes. *Vadose Zone J.* **7**, 587–600. https://doi.org/10.2136/vzj2007.0077 (2008).
23. Yang, Y. L. et al. The applicability of HYDRUS-1D to infiltration of water-repellent soil at different depths. *Eur. J. Soil. Sci.* **72**, 2020–2032. https://doi.org/10.1111/ejss.13100 (2021).
24. Dong, W., Wen, C., Zhang, P., Su, X. & Yang, F. Soil water and salt transport and its influence on groundwater quality: A case study in the Kongque river region of China. *Pol. J. Environ. Stud.* **28**, 1637–1650. https://doi.org/10.15244/pjoes/89610 (2019).
25. Jiang, J., Feng, S., Huo, Z., Zhao, Z. & Jia, B. Application of the SWAP model to simulate water–salt transport under deficit irrigation with saline water. *Math. Comput. Model.* **54**, 902–911. https://doi.org/10.1016/j.mcm.2010.11.014 (2011).
26. Zhang, P. & Shen, J. Effect of brackish water irrigation on the movement of water and salt in salinized soil. **14**, 404–413, doi: (2022). https://doi.org/10.1515/geo-2022-0367

27. Gharbia, A. S. Balázs zákányi, and Márton tóth. Impact of sand media continuous drying and rewetting Cyclic on nutrients transformation performance from reclaimed wastewater effluent at soil aquifer treatment. *Sci. Rep.* **14** (1), 8065 (2024).
28. van Genuchten, M. T. A Closed-form equation for predicting the hydraulic conductivity of unsaturated soils. *Soil Sci. Soc. Am. J.* **44**, 892–898. https://doi.org/10.2136/sssaj1980.03615995004400050002x (1980).
29. Liu, H. et al. Effect of median Soil–Particle size ratio on water storage capacity of capillary barrier. *Water.* **16**(13), (2024).
30. Kumar, V., Chaplot, B., Omar, P. J., Mishra, S. & Md. Azamathulla, H. Experimental study on infiltration pattern: opportunities for sustainable management in the Northern region of India. *Water Sci. Technol.* **84**, 2675–2685. https://doi.org/10.2166/wst.2021.171 (2021).
31. Chen, M., Mei, J., Shen, K. & Gao, Y. Response of sandy Soil–Water migration to different conditions under unidirectional freezing. *Sustainability.* **16**(9), (2024).
32. Fang, Y. W., Huanng, N., Bi, M. X. Y., Zhan, W. X. & G. Q. & The applicability of HYDRUS-1D to infiltration of water-repellent soil at different depths [J]. *Eur. J. Soil. Sci.* **48**, 193–200. https://doi.org/10.13758/j.cnki.tr.2016.01.029 (2016).
33. Zhang, Y., Wang, Y., Shah, K. F. & Li, T. Moisture stabilization of embankment subgrade with capillary barrier cover under dry and rainy weathers. *Transp. Geotechnics.* **42**, 101057. https://doi.org/10.1016/j.trgeo.2023.101057 (2023).
34. Liu, H. et al. Influence of interlayer soil on the water infiltration characteristics of heavy Saline–Alkali soil in Southern Xinjiang. *Agronomy.* **13**(7), (2023).
35. Liu, H. B. et al. *Appl. Ecol. Environ. Res.* **22**, 777–794, doi:https://doi.org/10.15666/aeer/2201_777794 (2024).
36. Shainberg, I., Rhoades, J. D. & Prather, R. J. Effect of low electrolyte concentration on clay dispersion and hydraulic conductivity of a sodic soil. *Soil Sci. Soc. Am. J.* **45**, 273–277. https://doi.org/10.2136/sssaj1981.03615995004500020009x (1981).
37. Awedat, A. M., Zhu, Y., Bennett, J. M. & Raine, S. R. The impact of clay dispersion and migration on soil hydraulic conductivity and pore networks. *Geoderma* **404**, 115297. https://doi.org/10.1016/j.geoderma.2021.115297 (2021).
38. Yang, K. Study on the process of variable saturation infiltration caused by suspension clogging in farmland drainage and recharge, (2024).
39. Sun, X. Effects of salinity, pH and N application on N$_2$O emission from saline-alkali soil, (2014). (In Chinese)
40. Chen, H. et al. Significant response of microbial community to increased salinity across wetland ecosystems. *Geoderma* **415**, 115778. https://doi.org/10.1016/j.geoderma.2022.115778 (2022).

Acknowledgements

Author contributions

SY Chen, Y Ke, G Zhangconceived the idea of the study and wrote the manuscript; X Zhang, WY Zhang carried out data collection and analysis; YX Chen, ZJ Sang contributed valuable analysis and manuscript review; all authors approved the final manuscript.

Funding

Declarations

Competing interests

The authors declare no competing interests.

Additional information

Correspondence and requests for materials should be addressed to G.Z.

Reprints and permissions information is available at www.nature.com/reprints.

Publisher's note Springer Nature remains neutral with regard to jurisdictional claims in published maps and institutional affiliations.